MODELLING GEOTHERMAL CIRCULATION IN A "TVZ-LIKE" SETTING

David Dempsey[1], Julie Rowland[2], Rosalind Archer[1] and Susan Ellis[3]

[1]Department of Engineering Science, University of Auckland, Private Bag 92019, Auckland, New Zealand

[2]School of Environment, University of Auckland, Private Bag 92019, Auckland, New Zealand

[3]GNS Science, 1 Fairway Drive, PO Box 30-368, Lower Hutt, New Zealand

d.dempsey@auckland.ac.nz

Keywords: *Computational model, deep circulation, recharge, field evolution.*

ABSTRACT

Heat is transported through the brittle crust of the Taupo Volcanic Zone (TVZ) by up-flow of hot fluid through more than 20 distinct convective plumes, the locations of which depend upon prevailing permeability and temperature conditions. Complete knowledge of such conditions would greatly assist modelling studies investigating deep circulation or field evolution over geological time; processes that are typically impenetrable to direct surface observation. In practice, data are available only for the near surface, and, for depths greater than 2 km, estimates of temperature and permeability are largely inferred or reasoned.

In this paper we detail a 3-D numerical model for geothermal circulation in a rifted setting, in which heat is transported through a 50 x 80 km region by numerous convection cells. The model describes statistical properties of the TVZ, matching average values or distributions of geophysical observables, such as heat output across the rift, the average dimensions and properties of geothermal fields, etc. This approach permits permeability properties and temperature boundary conditions to be specified stochastically, i.e., by an average value about which some degree of spatially correlated fluctuation is permitted.

The resulting model reproduces the average surface heat output of 0.6-0.8 W m^{-2} and an across strike bimodal heat distribution consistent with the TVZ. Fluid flow paths indicate that recharge is sourced from an area 5-10 km distant from the field boundary, in which fluids slowly percolate to depths of 3-7 km before rapidly ascending to the surface. Return times vary widely both within and between fields but average 10-30 kyr, of which the final 25% represents buoyant upwelling of the fluid.

Over a period of 300 kyr field boundaries, as demarcated by contours of heat flow, are observed to migrate several km. Assuming distributions of hydrothermal alteration, and thus resistivity modification, correlate to regions of past and present upflow, we are able to juxtapose the current distribution of geothermal activity upon a historical context.

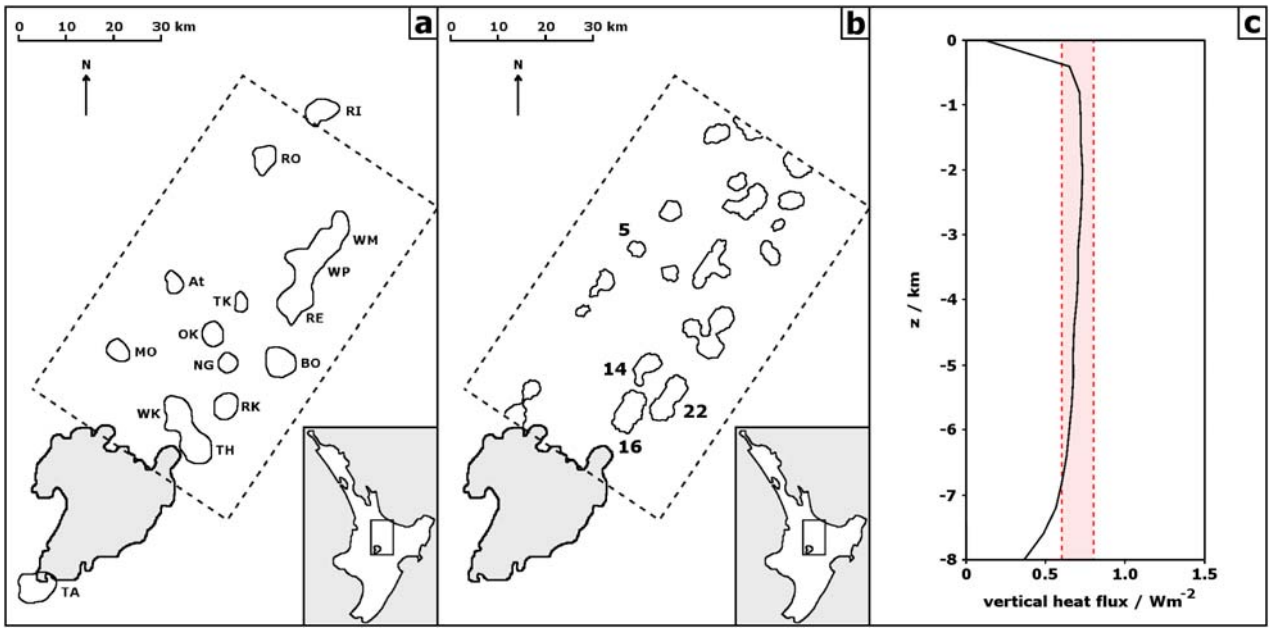

Figure 1: (a) Locations of geothermal fields within the TVZ and model domain (dashed outline). At = Atiamuri, BO = Broadlands-Ohaaki, MO = Mokai, NG = Ngatamariki, OK = Orakeikorako, RE = Reporoa, RI = Rotoiti, RK = Rotokawa, RO = Rotorua, TA = Tokaanu, TH = Tauhara, TK = Te Kopia, WK = Wairakei, WM = Waimangu, WP = Waiotapu. (b) Modelled geothermal fields after 190 kyr simulation time, delineated by the 0.1 W m^{-2} contour of vertical heat flux. Several fields are numbered and referred to in the text. (c) Mean vertical heat flux over the model domain with depth. Target interval from Hochstein (1995) shaded red.

1. INTRODUCTION

Beyond the limit of drilling, structural and circulation properties of the TVZ crust must be estimated either from indirect geophysical measurements (Bryan et al., 1999; Heise et al., 2008) or theoretical considerations (Bibby et al. 1995). Numerical modelling provides an additional tool for investigating the deep properties of the crust and the geothermal circulation it hosts. The rationale is that by reconstructing a system that faithfully describes observable sections of the crust, we also describe unknown regions or properties to some degree of accuracy.

Previous modelling studies of the TVZ have considered the full convective system (e.g., Kissling and Weir, 2005) or more directed investigations of specific reservoirs, notably Wairakei-Tauhara (Mannington et al., 2004; O'Sullivan et al., 2009). These studies demonstrate the capacity of models to match geophysical data and make subsequent observations or inferences on the future response of the system.

The purpose of this work is to model fluid recirculation within a permeable crust heated from below. The model reproduces a system of convective cells that have similar properties to those in the TVZ. Once the circulation model is established to an acceptable level of accuracy, we are able to investigate fluid flow paths through the deep crust. We also examine the spatial stability of geothermal fields through surface observations over a 300 kyr time period.

2. MODEL SETUP

This study seeks to reproduce a system of convective cells that are statistically consistent with those in the central TVZ. Figure 1(a) shows the target region, 50 km across and 80 km along strike, beginning at the northern end of Lake Taupo and encompassing 13 geothermal fields. The model domain extends to 8 km depth, which is the approximate base of the brittle crust and the estimated limit of fracture permeability (Bryan et al., 1999). Geothermal circulation is simulated for a period of 500 kyr on a structured mesh with horizontal and vertical nodal spacing of 500 and 400 m respectively. Simulations are performed using the Finite Element Heat and Mass transfer (FEHM) code (Zyvoloski et al., 1988).

Convective circulation is generated by the application of an across-strike, piece-wise temperature boundary condition at the base of the model. Figure 2(b) shows this is comprised of a low temperature background (225°C) at the margins of the rift, a warmer hotplate between 10 and 27.5 km (280°C), and a high temperature hotplate between 27.5 and 40 km (340°C). These conditions have been selected to generate an across-strike heat output that is approximately consistent with the bimodal distribution observed for the TVZ (Bibby et al., 1995; see Figure 2(a)).

Permeability structure plays an important role in determining heat output and dimensional characteristics of individual and the ensemble of convection cells. For these simulations we consider several geophysical criteria in constructing a permeability distribution, including: a surface layer of permeable volcanic strata; decaying permeability due to fracture closure with depth; and a spatially correlated fluctuation field that captures the stochastic nature of fracture distribution in the crust.

The average vertical permeability at the surface of the rift (defined as $5 < x < 45$ km) is 10 mD, representing high porosity volcanic deposits to a depth of 2 km. Below 2 km

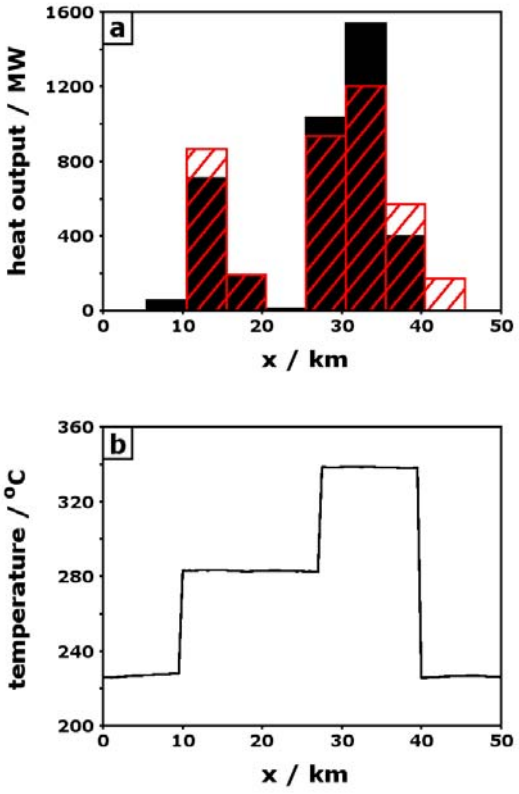

Figure 2: (a) Model across strike heat distribution binned every 5 km (black) compared to TVZ distribution (red, from Bibby et al. (1995)). For the purposes of comparison model data has been scaled to match total heat output of Bibby et al. (1995). (b) Mean across strike temperature boundary condition at 8 km depth.

permeability decays exponentially until it is reduced by an order of magnitude (see Figure 3(a)). For the prescribed temperature boundary conditions this permeability distribution permits a mean vertical heat flux of 0.7 W m^{-2} (see Figure 1(c)), which is consistent with bounds suggested by Hochstein (1995).

Permeability outside the rift is two orders of magnitude less than its value inside, where tectonic extension presumably maintains extensional and shear fracturing. Horizontal permeability is everywhere three times as large as the vertical permeability.

Superimposed on the background permeability distribution is a spatially correlated field of deviations from the mean permeability. These represent natural fluctuations in the intensity and conductivity of fractured rock for crust near a state of 'criticality' (Leary, 2002; Heffer, 2007). This stochastic permeability distribution is shown in Figure 3(b) at a depth of 400 m.

Mass transfer at the sides and base of the model is zero, which permits a complete description of the convective system but does not account for the effects of magmatic fluids (Giggenbach, 1995). Atmospheric temperature and pressure boundary conditions are imposed at the upper surface.

3. DESCRIPTION OF CIRCULATION

The distribution of geothermal fields after 190 kyr of simulation time is shown in Figure 1(a), juxtaposed against

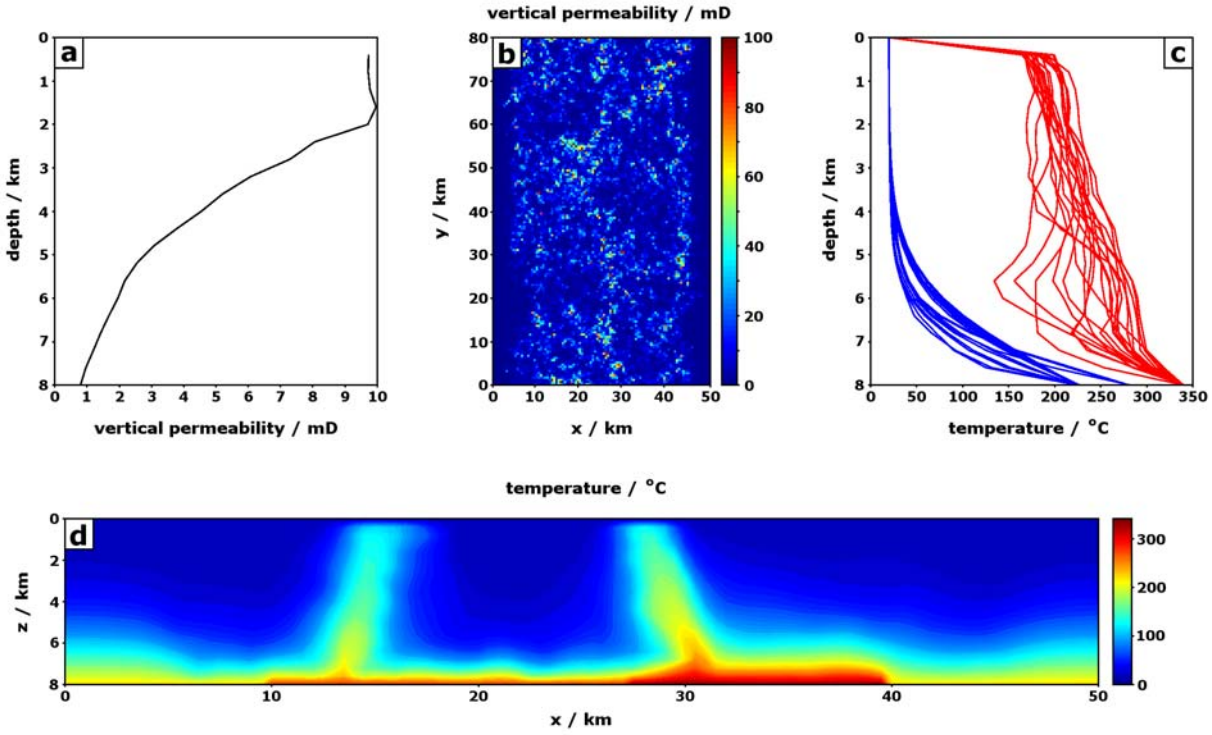

Figure 3: (a) Depth dependence of vertical permeability within the rift, i.e., 5 < *x* < 45 km. (b) Map view of spatially correlated permeability distribution at a depth of 400 m. (c) Vertical temperature profiles sited at the twenty highest (red) and twenty lowest (blue) recorded surface temperatures. (d) Temperature contours for a vertical slice at *y* = 56 km showing two deviated plumes.

the central TVZ. Qualitatively, modelled fields show similar size and spacing to their TVZ counterparts, although a precise judgment is challenging as resistivity (TVZ) and heat flow (model) contours are not necessarily directly comparable. In addition, interaction of hot upwelling fluids with surface hydrological processes and the subsequent effects on field shape and size have not been considered here.

Maximum surface temperatures (i.e., within 1 km of the surface) within the model fields are 185 – 215°C, which is cooler than those within the TVZ (approximately 250°C). This might be corrected by reducing the vertical dimension of the model, thereby bringing the hot basal temperature boundary condition closer to the surface. Alternatively, the isothermal character of upwelling fluid may be improved with the enforcement of an 'outflow boundary condition', i.e., dT/dz = 0 for upflow and T = 20°C for downflow (Jupp and Schultz, 2000).

Rapid temperature changes are observed in the surface boundary layer above geothermal plumes. Below this layer, temperature profiles in Figure 3(c) indicate that rising fluids cool by approximately 100°C. Several of these profiles show a temperature inversion near the base of the model where cold recharge is entrained into the base of the plume. These profiles are indicative of deviated plumes (Figure 3(d)), in which hot fluids rise along sub-vertical paths. In this case the divergence is an indication of a non-stationary plume (see section 5).

Recharge by downward percolation of cold fluids occurs throughout 85% of the rift (5 < *x* < 45 km). In many locations these fluids suppress the natural geothermal gradient to several km (see Figure 3(c)). The extent to which surface temperatures penetrate the crust was shown by Weir (2009) to be a function of the downward percolation velocity, v_d. In our model v_d has a mean of value of 0.8×10^{-9} m s^{-1}, which is similar to the infiltration rate of rainwater used in other models (Kissling, 2004; Weir, 2009).

4. DEEP FLOW

Reasonable constraints exist for the circulation of fluids, in the upper 1-2 km of the crust, in large part due to the abundance of well data. Beyond the reach of drilling, flow characteristics must be constrained by alternative methods, including geochemical investigations (Giggenbach, 1995) and physical considerations (Bibby et al., 1995; Weir, 2009). In this section we trace the flow paths of waters infiltrating the surface, percolating to the base of the convective system, and rising buoyantly within plumes.

A flow path, **x**, for some packet of fluid travelling through the crust is found by integrating its velocity, **v**, in time, i.e.,

$$\mathbf{x}(t) = \mathbf{x}_0 + \int_0^t \mathbf{v}(\mathbf{x}(\tau), \tau) d\tau \,. \qquad (1)$$

In practice **v** varies continuously in space and time, however model output is restricted to discrete positions (the nodes) and time steps. Here we have used a linear interpolation to calculate the velocity field at time, τ, between two time steps, τ_i and τ_{i+1}, and at position, **x**,

within a cuboid volume defined by eight nodes at positions, $\mathbf{x}_{1,2,\ldots 8}$. The integral in Equation (1) is discretized and calculated for advancing time steps Δt = 160 yr. For representative fluid velocities the flow path, $\mathbf{x}(t)$, is advanced in increments of 5-50 m, which is significantly less than the minimum node spacing (400 m).

Recharge characteristics for three fields in close proximity to each other are shown in Figure 4. For each field an ensemble comprising 5-10 thousand flow paths was constructed. Flow paths terminating within a specific field are generated by selecting a random $\mathbf{x}_0$ within that field and running Equation (1) backward in time, i.e., by setting Δt = -160 yr. The three fields are denoted 14, 16 and 22 and have, respectively, heat outputs of 85, 190 and 125 MW, and areas of 27, 48 and 49 km^2.

Our results indicate that downward percolation of fluids recharging these three fields is restricted to a square area of dimensions 25×25 km. Fluids circulate to a depth of between 2 and 8 km prior to becoming entrained in the upflow zone. The subsequent return journey to the surface is relatively rapid, and accounts for, on average, 25% of the return time, i.e., the total time taken for a round trip.

4.1 Fluid return characteristics

Distributions of return times for the three fields, shown in Figure 4(b), indicate that a given packet of fluid may spend between 5 and 100 kyr in transit through the crust. This spread is due, in part, to the variety of depths to which the recharging fluids penetrate. For a given average fluid velocity, return time is proportional to the length of the flow path, which itself depends on the penetration depth of fluid. Therefore in general, the further a packet of fluid travels the longer it must spend in transit.

The mean return times for fields 14, 16 and 22 are, respectively, 26, 21 and 31 kyr. In addition, field 22 exhibits two distinct upflow zones centred at y = 25 km and y = 18 km, for which the mean return times are 27 and 35 kyr, respectively. In contrast, Stewart (1978) estimated the age of deep geothermal water at Wairakei as less than 12 kyr, based on the absence of a glacial signal in their isotopic composition.

Return time is inversely proportional to the mean fluid particle velocity, defined as the Darcy velocity divided by porosity. Return time thus correlates negatively with permeability, k, (through the Darcy velocity) and positively with porosity, φ. Physically, larger values for k permit faster fluid velocities, but larger φ promotes a longer time spend 'in residence' within a pore. In practice, k and φ may be correlated such that residence time can be expressed as a function of k only. For rocks in which permeability is dominated by connected pore space, $k \propto \varphi^3$ is an appropriate relationship (Zhang et al., 1994), for which return time, t_{ret} depends negatively on k, i.e., $dt_{ret}/dk < 0$. Alternatively, for fracture dominated permeability, $\varphi \propto \log(k)$ (Leary and Al-Kindy, 2002), which produces return

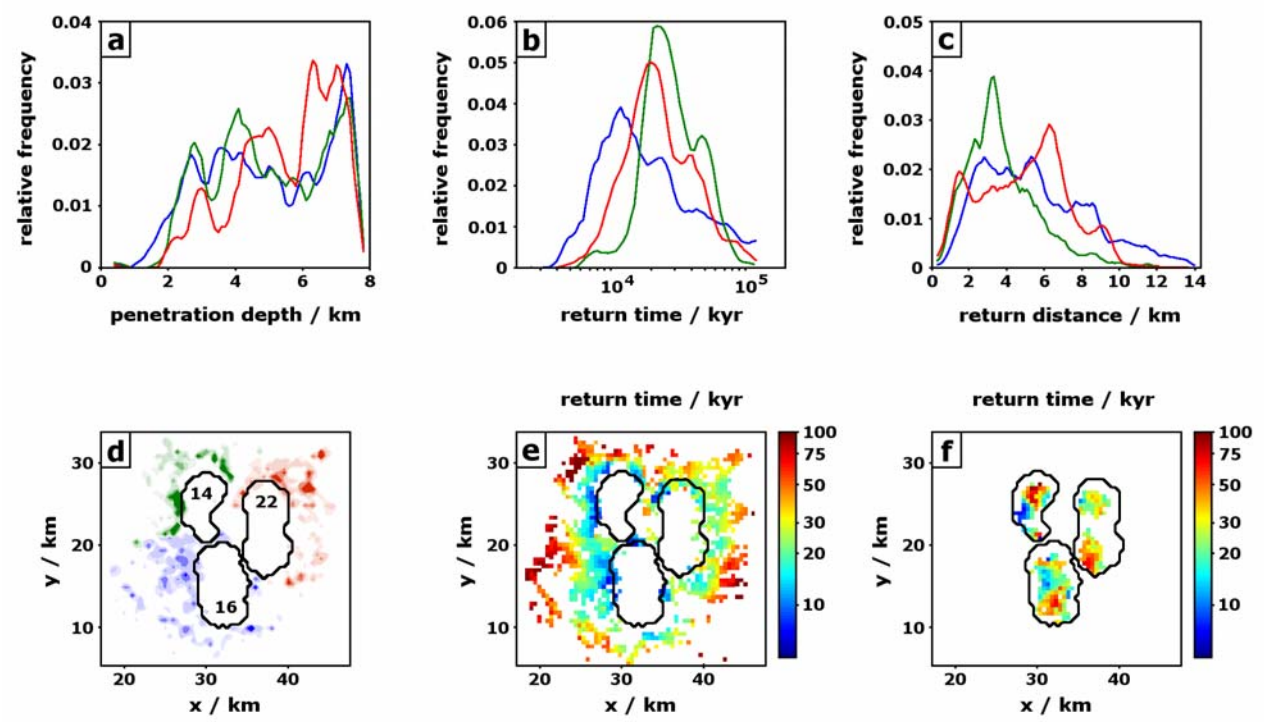

Figure 4: Recharge characteristics for three neighboring plumes (see Figure 1(b) for regional context). Relative frequency plots for (a) maximum penetration depth of flow paths, (b) return time, i.e., time taken to return to surface, and (c) return distance, i.e., horizontal distance travelled by fluids upon return to surface. Profiles for fields 14, 16 and 22 are coloured green, blue and red respectively. (d) Relative frequency contours indicating areas of recharge. Each of the numbered fields has an exclusive zone of recharge, with darker colours indicating a greater proportion of the recharge derived from that area. Field colour correspondence as in (a-c). Black lines indicate field boundary. (e) Mean return time at point of infiltration for the three fields. White areas indicate insufficient data, i.e., fluids infiltrating here do not exit from fields 14, 16 or 22. (f) Mean return time at point of expulsion.

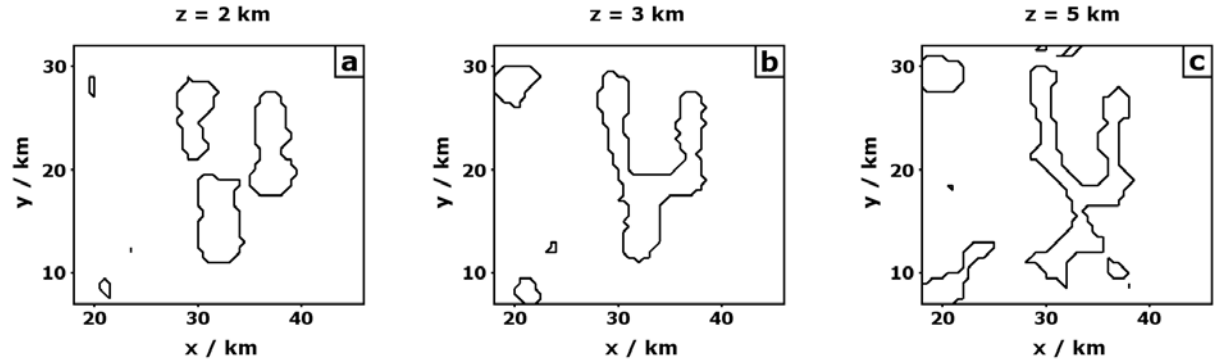

Figure 5: Vertical heat flux contours for 0.1 Wm^{-2} at depths of (a) 2, (b) 3, and (c) 5 km. For the purposes of comparison horizontal slices are positioned approximately below those in Figure 4(d-f).

times that depends positively on k, i.e., $dt_{ret}/dk > 0$.

Figure 4(e) plots the mean return time for fluids entering the crust at a given location and indicates that older fluids are, in general, sourced at greater distances from geothermal fields. Less intuitively, Figure 4(f) shows that mean age of fluids exiting within a field varies considerably with position. For instance, field 14 exhibits mean return times of 10 kyr and 100 kyr separated by a distance of only 3 km. This variety in age implies an associated variety in source waters for fluids exiting within a given field.

Return distance for a given flow path, which we define as the horizontal distance travelled by recharging fluids upon their return to the surface, ranges from 2-15 km (see Figure 4(c)) depending on the field. This indicates that recharging fluids are drawn from a limited area proximate to the field, although not necessarily from a symmetrical 'halo'. Figure 4(d) shows that feeder zones for each of the three fields occupy distinct regions with minimal overlap. Further, within each feeder zone there exist regions of greater and lesser contribution to the total recharge.

4.2 Plume structure at depth

Fields 14, 16 and 22, which present as distinct zones of vertical heat flow at the surface, exhibit some connection at depth. Figure 5 shows the 0.1 W m^{-2} heat flux contour (used to delineate field boundaries in Figure 1(b) and 4(d-f)) at depths of 2, 3 and 5 km. The three fields remain disconnected to a depth of 2 km only, below which fields 14 and 22 develop bridges to field 16 that persist to a depth of 5 km. However, to assert a hydrological connection between these fields would imply some mixing of their respective source fluids. This is not supported by Figure 4(d), which shows no overlap between feeder zones for the three fields, except for a small region between zones 14 and 16. Pressure communication between the fields may represent an alternative mode for hydrological connection, however this scenario is not considered here.

Interpretation of plume structure at depth depends on the specific parameter being used to constrain its shape. Figure 6 presents three such options: (a) vertical heat flux, (b) temperature, and (c) density, for field 5 (see Figure 1(b)), a low temperature field producing 45 MW of heat over an area of 12 km^2. Isosurfaces of heat flux for this field indicate that heat is transported vertically through the crust via discrete pipe structures. The 1 W m^{-2} isosurface sufficiently constrains the conduit and heat transport is proportionally greater as distance from the axis of flow is reduced. The maximum heat flux obtained within the upwelling column is approximately 10 W m^{-2}; however this is expected to scale positively for larger fields. Heat transport within the 1 W m^{-2} isosurface is approximately

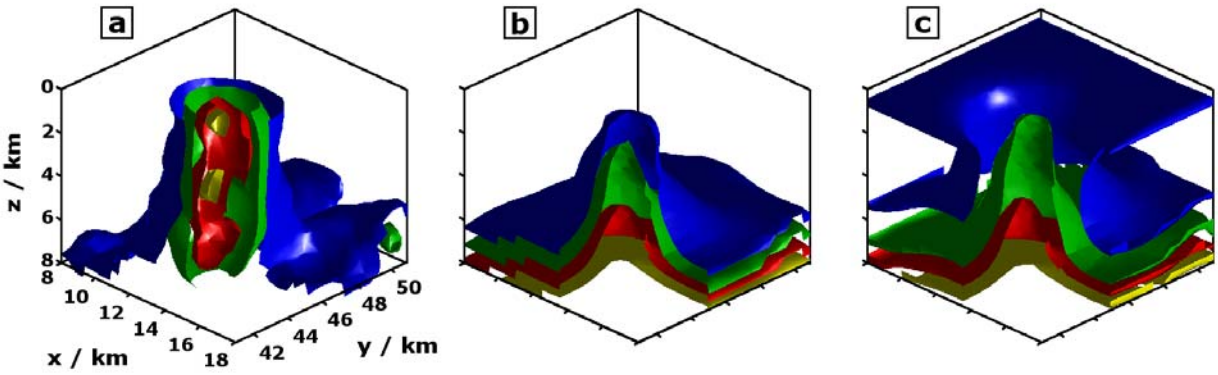

Figure 6: Isosurfaces for a low temperature field in the cooler region of the model, i.e., 10 < x < 27.5 km. (a) Vertical heat flux drawn at levels 0.1 (blue), 1 (green), 5 (red) and 10 W m^{-2} (yellow). (b) Temperature drawn at levels of 100 (blue), 150 (green), 200 (red) and 250 °C (yellow). (c) Fluid density drawn at levels of 1000 (blue), 950 (green), 900 (red) and 850 kg m^{-3} (yellow). Vertical cuts have been made to excise a cubic region of data satisfying x > 13.3 km and y < 45.5 km.

adiabatic as fluid is transported from the base of the plume to the surface.

Contours of temperature and density indicate that fluids become cooler and denser as they rise through the plume. For depths over which fluids ascend adiabatically, gradients of temperature and density along the axis of the plume are approximately constant at 19 °C km^{-1} and 14 kg m^{-3} km^{-1}, respectively. Qualitatively, the plume appears as a series of concentric, overlain Gaussian surfaces rather than a pipe-like conduit.

Outside the plume, Figure 6(c) exhibits an inversion in the vertical density gradient, dρ/dz, of the recharging fluids. Figure 3(c) shows that descending fluids do not increase in temperature appreciably until approximately 5 km depth, i.e., the onset of the lower boundary layer. Above this depth density changes are induced by increasing hydrostatic pressure, such that a maximum density of 1010 kg m^{-3} is achieved at a depth of approximately 3.5 km. Below this depth, the temperature gradient is large enough that density reductions with increasing temperatures exceed density increases with increasing pressure. Mathematically this is expressed

$$\frac{d\rho}{dz} = \frac{\partial\rho}{\partial T}\frac{dT}{dz} + \frac{\partial\rho}{\partial P}\frac{dP}{dz} < 0, \qquad (2)$$

where ρ is fluid density, *T* is temperature and *P* is pressure. An inversion in the density gradient then occurs when the temperature term in Equation (2), which is negative, exceeds the pressure term in magnitude, which is positive.

5. EVOLUTION OVER GEOLOGICAL TIME

The stability of TVZ geothermal fields is commonly judged by their age and ability to endure volcanic activity. Minimum age estimates range from 500 kyr for Wairakei, 400 kyr for Ngatamariki (Arehart et al., 1997), and 200 kyr for Kawerau (Browne, 1979). In addition, both Wairakei and Waimangu geothermal fields appear to have maintained activity during recent volcanism, albeit with significant changes to surficial features for the latter.

In the previous sections we have described the state of geothermal circulation at a given point in time, i.e., after 190 kyr of simulation time. The modelled heat flow distribution and individual field characteristics at this time are consistent with TVZ observations, suggesting the model is making some approximation to the current state of the TVZ. However, during the 310 kyr of simulation time that

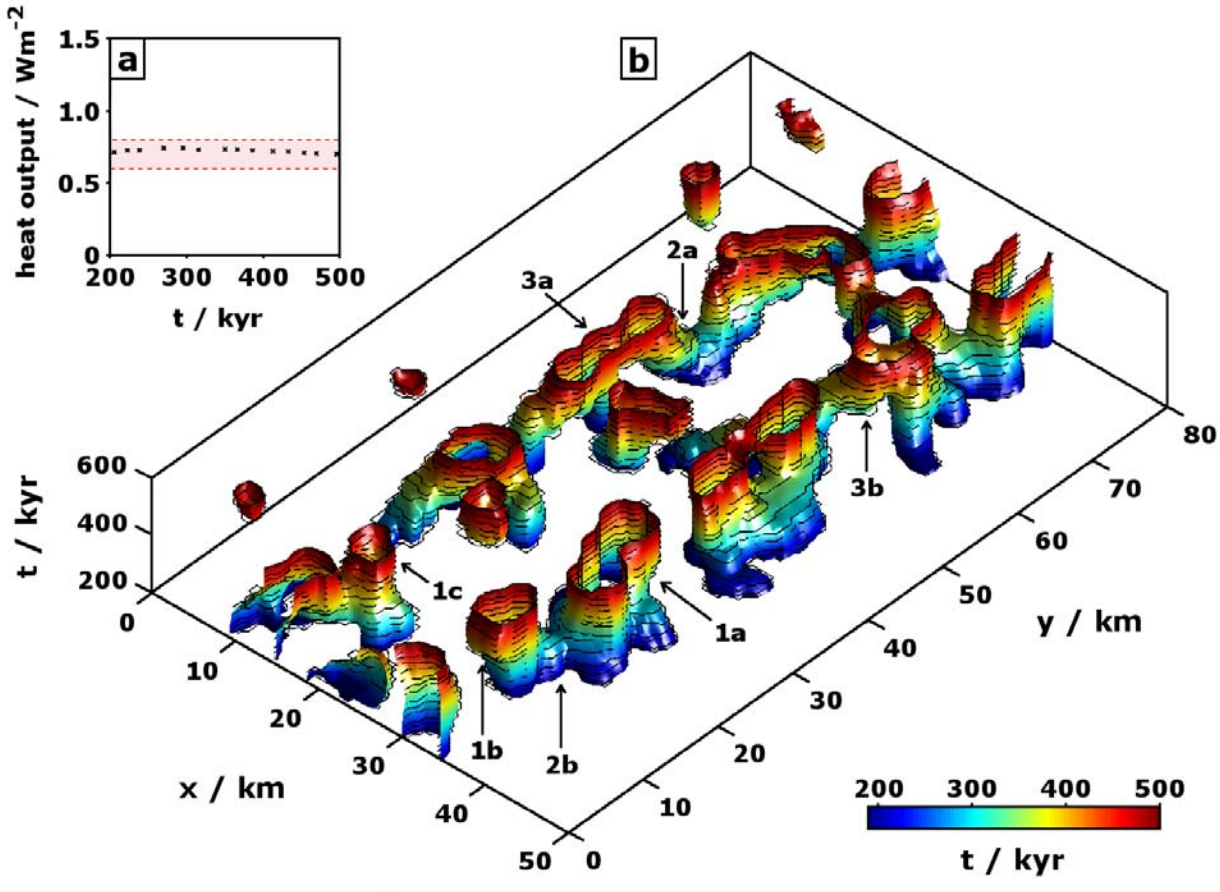

Figure 7: (a) Mean vertical heat flux through the crust (1 < z < 7 km) over 300 kyr of simulation time. Target interval from Hochstein (1995) is shaded red (c.f. Figure 1(c)). (b) Evolution of field positions and dimensions over 300 kyr of simulation time. Isosurfaces contour 1 Wm^{-2} vertical heat flux over 14 simulation time steps (vertical axis). Isosurface colour corresponds to age (and thus vertical axis). Black contours indicate raw data from which surfaces are interpolated. Field positions in 1(b) correspond to the lowest level of the figure. Labels 1a-c, 2a-b, and 3a-b are referred to in the text.

follow, significant movement in the positions of fields is observed, despite a steady average heat output of the rift (Figure 7(a)).

Figure 7(b) plots the evolving positions of geothermal fields at the surface of the model using the vertical axis and colour to represent simulation time. In this representation field boundaries are denoted in the horizontal plane by the 1 Wm^{-2} vertical heat flux contour for that time step. For a field that does not change position in time, subsequent contours would plot immediately above one another and an isosurface plotted through these would yield a vertical column. Several such structures are identified in Figure 7(b) (marked 1a-1c) and represent field stability over periods of 100-300 kyr.

In contrast to the relative stability of these fields, the majority of fields exhibit a degree of transience, which manifests as a horizontal component of the isosurface. In several instances (Figure 7(b), 2a-2b) fields split in two, with diverging components migrating away from one another at rates of up 1-2 km per 100 kyr. The complementary process in also observed, i.e., two or more smaller fields migrating towards one another and eventually merging into larger structures (e.g., Figure 7(b), 3a-3b).

Figure 8 plots the time since hydrothermal circulation has been hosted at the surface of the model, and therefore shows the final distribution of geothermal fields (red) in the context of previous circulation (other colours). We observe that for many fields upflow has previously occurred outside their present boundary. However, over geological time scales the region influenced by a given field, i.e., that region including past and present activity, is limited in extent. Within the TVZ, regions of previous hydrothermal circulation are frequently inferred from alteration of the rock and its subsequent effect on resistivity (Risk et al., 1994). Figure 8 is then somewhat analogous to a resistivity map, albeit one that documents the age, rather than extent, of alteration. It further suggests that field boundaries demarcated by resistivity contours (past and present circulation), do not necessarily correspond to field boundaries constrained by heat flux.

Figure 8 also shows large tracts of the crust have remained free from geothermal activity over geological time scales. In particular, a narrow corridor along the line x = 25 km, corresponding to the central minimum in Figure 2(a), appears to function as a recharge zone for geothermal activity either side. This region thus approximates, in both position and function, the Taupo Fault Belt (TFB), which traverses the central TVZ from the north of Lake Taupo through to the Okataina Volcanic Centre. Widespread and active normal faulting within the TFB is expected to enhance fracture permeability to seismogenic depths. This assumption has been incorporated into previous circulation models (Kissling and Weir, 2005) resulting in a preference for downflow in this region. However, in our model no special permeability conditions are required to keep this region free of hydrothermal activity. Rather, downflow occurs preferentially along the central axis a consequence of the wider circulation system that develops in response to the prescribed thermal boundary conditions.

6. CONCLUSION

A 3-D model for geothermal circulation within a crust constrained by TVZ realistic parameters has been detailed.

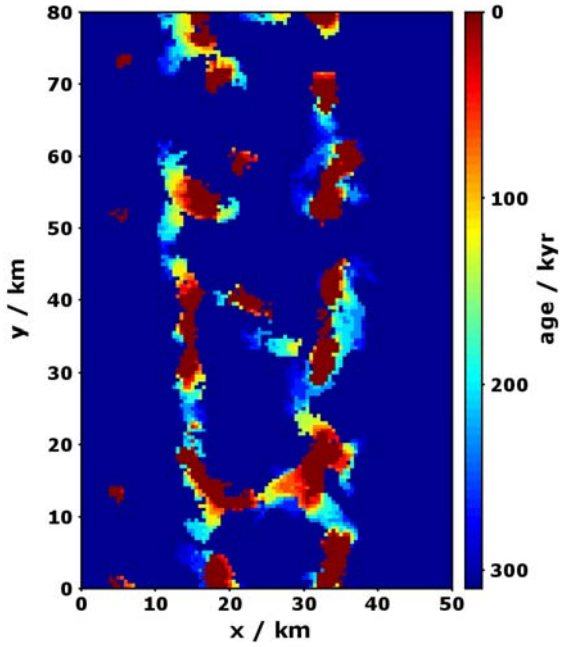

Figure 8: Age of geothermal circulation at the surface.

The central TVZ region, which encompasses the majority of geothermal activity, is modelled to a depth of 8 km, with convection driven by temperature boundary conditions imposed at the base. Outside the rift, basal temperatures are too cool for convective transport, while within the rift a two-temperature hot plate is imposed. The result is a bimodal across strike heat distribution that is qualitatively similar to that observed for the TVZ. It includes an enhanced heat output along the western side of the model, and an anomalously low heat output through the central sections. This low heat zone functions primarily as a recharge zone for neighbouring fields and is analogous to the Taupo Fault Belt within the TVZ.

We have calculated ensembles of fluid flow paths to explore and constrain the downflow of rainwater that recharges individual fields. Our results indicate that fluids percolate to a range of depths in the crust prior to their entrainment in the upflow zone of a convection cell. These fluids are sourced from up to 10 to 15 km from a field's boundary and may derive from preferred directions depending on the proximity of neighbouring fields. The model suggests that recharging fluids may spend several 10's of kyr in transit through the crust, which is inconsistent with isotopic analysis of the age of waters from Wairakei geothermal field (Stewart, 1978), but may be improved through better constraints on porosity and permeability.

The spatial stability of geothermal fields in time has been investigated for an interval of 300 kyr. Over this period we observe moderate migrations of up to 5-10 km in the position of upflow zones. We also observe instances of fields splitting and following diverging migratory paths, or two fields converging into one larger field. In addition, we note a wide corridor corresponding to the long axis of the model that remains largely free of upflow for the term of the simulation.

The purpose of the model presented here is to approximate the TVZ in a statistical sense with only minimal constraint on the permeability distribution and thermal boundary

conditions. To this end, we have prescribed the statistics of permeability variability in space, rather than permeability directly, thereby avoiding an exhaustive search of the parameter space in an attempt to match model outflows to the TVZ. However, this approach places specific limits on the relevance of the model. In particular, little comment can be offered on specific fields within the TVZ, except where a modelled field is similar in size and output to a TVZ counterpart. In this case, estimates of return time or migratory behaviour may be applicable, although plume structure (Figure 6), distributions of feeder zones (Figure 4(d)), or age of upflow within a field (Figure 4(c)) would depend on the specific permeability distribution. Nevertheless, this approach to modelling has demonstrated some utility in describing the dynamics of fluid circulation within the TVZ. For instance, we have demonstrated a degree of spatial instability of the modelled fields, despite a static permeability distribution and basal temperature boundary conditions. We hope that further improvements to the model, such as dynamic permeability or a mixed atmospheric temperature boundary condition, will permit new insights in the future.

ACKNOWLEDGEMENTS

This research was funded by the Tertiary Education Commission, New Zealand through a Top Achievers Doctoral Scholarship and by an Energy Education Trust of New Zealand Scholarship. The authors wish to thank George Zyvoloski for supplying the FEHM fluid flow code and assisting in its implementation.

REFERENCES

Arehart, G. B., Wood, C. P., Christenson, B. W., Browne, P. R. L., Foland, K. A.: Timing of volcanism and geothermal activity at Ngatamariki and Rotokawa, New Zealand. *Proc. 19th NZ Geotherm. Workshop.* pp. 117-122. (1997)

Bibby, H. M., Caldwell, T. G., Davey, F. J., Webb, T. H.: Geophysical evidence on the structure of the Taupo Volcanic Zone and its hydrothermal circulation. *J. Volcan. Geotherm. Res.* v. 68, pp. 29-58. (1995)

Browne, P. R. L.: Minimum age of the Kawerau geothermal field, North Island, New Zealand. *J. Volcan. Geotherm. Res.* v. 6, pp. 213-215. (1979)

Bryan, C. J., Sherburn, S., Bibby, H. M., Bannister, S. C., Hurst, A. W.: Shallow seismicity of the central Taupo Volcanic Zone, New Zealand: its distribution and nature. *N. Z. J. Geol. Geophys.* v. 42, pp. 533-542. (1999)

Giggenbach, W. F.: Variations in the chemical and isotopic composition of fluids discharged from the Taupo Volcanic Zone, New Zealand. *J. Volcan. Geotherm. Res.* v. 68, pp. 89-116. (1995)

Heffer, K. J.: Proximity to a critical point: evidence from, and implications for, hydrocarbon reservoirs. *Geol. Soc. Lon. Spec. Pub.* v. 289, pp. 227-239. (2007)

Heise, W., Caldwell, T. G., Bibby, H. M., Bannister, S. C.: Three-dimensional modelling of magnetotelluric data from the Rotokawa geothermal field, Taupo Volcanic Zone, New Zealand. *Geophys. J. Int.* v. 173, pp. 740-750. (2008)

Hochstein, M. P.: Crustal heat transfer in the Taupo Volcanic Zone (New Zealand): comparison with other volcanic arcs and explanatory heat source models. *J. Volcan. Geotherm. Res.* v. 68, pp. 117-151. (1995)

Jupp,T., Schultz, A.: A thermodynamic explanation for black smoker temperatures. *Lett. Nat.* v. 403, pp. 880-883. (2000)

Kissling, W. M.: Large-scale hydrology of the Taupo Volcanic Zone, New Zealand. PhD thesis, Auckland University. (2004)

Kissling, W. M., Weir, G. J.: The spatial distribution of the geothermal fields in the Taupo Volcanic Zone, New Zealand. *J. Volcan. Geotherm. Res.* v. 145, pp. 136-150. (2005)

Leary, P. C.: Fractures and physical heterogeneity in crustal rock, *in* Goff, J. A., and Hollinger, K., eds., Heterogeneity in the crust and upper mantle: Nature, scaling and seismic properties. New York, Kluwer Academic, pp. 155-186. (2002)

Leary, P. C., Al-Kindy, F.: Power-law scaling of spatially correlated porosity and log(permeability) sequences from north-central North Sea Brae oilfield well core. *Geophys. J. Int.* v. 148, pp. 426-442. (2002)

Mannington, W., O'Sullivan, M., Bullivant, D.: Computer modelling of the Wairakei-Tauhara geothermal system, New Zealand. *Geothermics*. v. 33, pp. 401-419. (2004)

O'Sullivan, M. J., Yeh, A., Mannington, W. I.: A history of numerical modelling of the Wairakei geothermal field. *Geothermics*, v. 38, pp. 155-168. (2009)

Risk, G. F., Caldwell, T. G., Bibby, H. M.: Deep resistivity surveys in the Waiotapu-Waikite-Reporoa region, New Zealand. *Geothermics.* v. 23, pp. 423-443. (1994)

Stewart, M.: Stable isotopes in waters from the Wairakei geothermal area, New Zealand. *DSIR Bull.* v. 220, pp. 113-119. (1978)

Weir, G. J.: A mathematical model of rainfall-controlled geothermal fields. *Transp. Porous Med.* v. 77, pp. 323-334 (2009)

Zhang, S., Paterson, M. S., Cox, S. F.: Porosity and permeability evolution during hot isostatic pressing of calcite aggregates. *J. Geophys. Res.* v. 99, pp. 15,741-15,760. (1994)

Zyvoloski, G., Dash, Z. V., and Kelkar, S.: FEHM: Finite Element Heat and Mass Transfer Code, *LA-12062-MS*. (1988)